

Experimental Observation of Nonlocal Electron Thermal Transport in NSTX RF-heated L-mode plasmas

Y. Ren¹, B. P. LeBlanc¹, W. Guttenfelder¹, S. M. Kaye¹, E. Mazzucato¹, K. C. Lee², C. W. Domier³, R. Bell¹, D. R. Smith⁴, H. Yuh⁵

¹Princeton Plasma Physics Laboratory, Princeton, NJ 08543

²National Fusion Research Institute, Daejeon, 305-333, Korea

³University of California at Davis, Davis, CA 95616

⁴University of Wisconsin-Madison, Madison, WI, 53706

⁵Nova Photonics, Inc., Princeton, NJ 08540

E-mail contact of main author: yren@pppl.gov

Abstract. In this paper, we report the first observation of nonlocality in electron thermal transport and turbulence in National Spherical Torus eXperiment (NSTX) [M. Ono et al., Nucl. Fusion 40 557, 2000]. The observation was made in a set of RF-heated L-mode plasmas with toroidal magnetic field of 5.5 kG and plasma current of 300 kA. It is observed that electron-scale turbulence spectral power (measured with a high-k collective microwave scattering system) is reduced significantly following the cessation of RF heating. The large drop in the turbulence spectral power has a time delay of about 1-2 ms relative to the RF cessation and happens on a time scale of 0.5-1 ms, much smaller than the energy confinement time of about 10 ms. Power balance analysis shows a factor of about 2 decrease in electron thermal diffusivity after the sudden drop of turbulence spectral power. This sudden reduction in the measured turbulence and the decrease in electron thermal transport cannot be explained by the expected small changes in local equilibrium profiles over the 0.5-1 ms time scale. This expectation is supported by equilibrium profile measurements across the RF cessation. The observation above demonstrates the nonlocal nature of the observed turbulence and electron thermal transport. Local linear gyrokinetic stability analysis shows that the changes in linear growth rates of ion and electron-scale instabilities across the RF cessation are not consistent with the observed drop in the measured turbulence spectral power.

1. Introduction

Understanding electron thermal transport is crucial for improving and predicting the confinement performance of future fusion devices, e.g. Fusion Nuclear Science Facility (FNSF) [1] and ITER. The observations of nonlocality in electron thermal transport and turbulence in tokamaks and stellarators [2,3] challenge the standard local model of transport and turbulence where transport coefficients are assumed to be functions of local mean thermodynamic quantities and their gradients. We note that this local transport paradigm is the basis for many present predictive codes. The experimental observations of nonlocality in electron thermal transport and turbulence usually involve measuring dynamic responses of plasma to a sudden change in heating power, either decrease or increase. For example, the earliest observation of nonlocal electron thermal transport was made by injecting carbon into tokamak edge plasmas to induce a sudden edge cooling [2]. The observation of an almost simultaneous rise in core electron temperature with respect to edge cooling cannot be explained under the local transport paradigm. Furthermore, the measured core density fluctuation amplitude showed no obvious change responding to the improved electron thermal confinement in the core. More recently, such edge cooling experiments were performed on Alcator C-Mod tokamak, where nonlocal electron thermal transport was observed in low collisionality linear Ohmic confinement regime but not in the high collisionality saturated Ohmic confinement regime [4]. These observations indicate the potential role of collisionality in parameterizing regimes of nonlocal electron thermal transport. In addition to edge cooling, core electron heating was also used to induce sudden change in electron heating [5]. The experiments with modulated Electron Cyclotron Heating (ECH) on Large Helical Device

(LHD) have shown that while measured turbulence almost immediately responds to the change in heat flux (due to ECH turn-on and off), the change in local Electron Temperature Gradient (ETG) is much slower. This observation shows that the local turbulence may not be solely determined by local thermodynamic quantities and their gradients, and that the observed electron thermal transport is clearly nonlocal. However, to the authors' knowledge, no observation of nonlocality in turbulence and electron thermal transport has been reported for a spherical tokamak. Furthermore, all previous observations only measured low- k and low frequency fluctuations. On the other hand, there is accumulated evidence that electron-scale (high- k) turbulence, i.e. ETG turbulence, can be important for driving anomalous electron thermal transport [6], particularly in spherical tokamaks [7,8] where low- k turbulence can be suppressed by ExB shear [9]. Thus how electron-scale (high- k) turbulence behaves when subjected to external perturbations is of great interest to study.

2. Experimental Apparatus

Figure 1 plots the scattering configuration of the high- k scattering system [10] used in the study presented in this paper, including the probe beam and scattered beam trajectories calculated using a ray tracing code. The five receiving channels cover a wavenumber range of $5 \text{ cm}^{-1} \lesssim k_{\perp} \lesssim 30 \text{ cm}^{-1}$ with a wavenumber resolution of about 1 cm^{-1} (k_{\perp} is the perpendicular wavenumber), and five heterodyne receivers allow us to distinguish the wave propagation direction for each different wavenumber. The power response of each receiving channel was calibrated with a solid-state microwave source with known output power. The frequency response of the scattering system is about 5 MHz. A radial resolution of $\Delta R \approx \pm 2 \text{ cm}$, determined by the $1/e$ half width of the microwave beam power, is the unique feature of the scattering system. This is made possible by the tangential launching scheme (see Fig. 1) along with the large toroidal curvature of NSTX due to its low aspect ratio, which leads to a scattering volume much smaller than that from the overlapping of the probe and scattering beams [11]. This fine radial resolution allowed us to study the dependence of locally measured turbulence on local equilibrium quantities, e.g. L_{T_e} [12] (electron temperature scale length), L_{n_e} [7,13] (electron density scale length), collisionality [13], q (safety factor), and \hat{s} (magnetic shear) [14]. Improvements in scattering scheme have significantly reduced stray radiation, which made it possible to obtain scattering signals from all five channels simultaneously, compared to at most three channels previously [15]. Remote control capability allowed between-shot adjustment of launching and receiving optics, which made it possible to optimize scattering configuration according to realized plasma equilibria. We note that due to the tangential launching scheme employed, the scattering system measures mostly radial wavenumber, k_r , and finite but smaller poloidal wavenumber, k_{θ} , e.g. a range of $k_r \rho_s \sim 1-9$ and a range of $k_{\theta} \rho_s \sim 2-3$ for the experiments presented in this

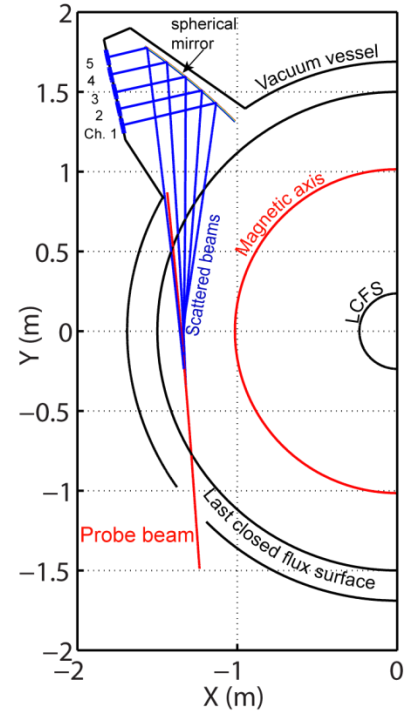


Figure 1 Schematic of the scattering configuration of the high- k scattering system used in the study presented in this paper. The probe beam and scattered beam trajectories are calculated using a ray-tracing code. Scattered light is reflected and focused by a spherical mirror onto five collection windows.

paper. We note that as shown in Fig. 1, the scattered beam to channel 5 is partially blocked by the vacuum vessel and thus is not used in the following analysis.

3. Results

Here, we present the first experimental observation of nonlocality in turbulence and electron thermal transport in National Spherical Torus eXperiment (NSTX) [16]. The observations were made at the times of RF cessation in a set of NSTX RF-heated L-mode plasma with $B_T=5.5$ kG and $I_p=300$ kA. Local electron-scale turbulence was measured the high- k scattering system and the scattering system was configured to measure turbulence for a $k_{\perp}\rho_s$ (ρ_s is the ion gyroradius at electron temperature) range of about 2 to 10 at the radial region of $R\approx 133$ to 137 cm ($r/a\approx 0.57-0.63$, named as the high- k measurement region). In the rest of this paper, we will present results from a typical shot 140301 for which we have carried out extensive analysis.

The correlation between the cessation of RF heating and the reduction in electron-scale turbulence is demonstrated in Fig. 2. Figure 2(a) shows that the peak injected RF power is about 1 MW and the RF heating terminates at $t=479.6$ ms (denoted by a vertical dashed line in Fig. 2). The maximum electron temperature, T_e , measured by a Thomson scattering system [17] is shown in Fig. 1(b), and it is clearly seen that the maximum T_e drops after RF heating terminates (the RF heating in NSTX provides core electron heating [18]). Figure 2(c) shows the spectrogram of the signal from channel 3 of the high- k scattering system, measuring to a normalized wavenumber $k_{\perp}\rho_s$ of about 4-5. The scattering signal, i.e. the spectral peaks at $f<0$ shown in Fig. 2(c), can be distinguished easily from the stray radiation, i.e. the central peak at $f=0$, from about $t=300$ ms to 550 ms, and we can see that a sudden drop in scattered signal power at almost the same time as the RF cessation at $t=479.6$ ms. This sudden drop is more clearly shown in Fig. 2(d) where the time trace of the peak spectral power of the scattering signal in Fig. 2(c) is shown. Note that the time trace in Fig. 2(d) is only shown from $t=300$ to 520 ms when the scattering signal, i.e. the spectral peak at $f<0$, can be clearly separated from the stray radiation, i.e. the central peak at $f=0$. To establish a causal relation between the RF heating cessation and the reduction in measured turbulence, a careful examine their temporal relation is shown as follows.

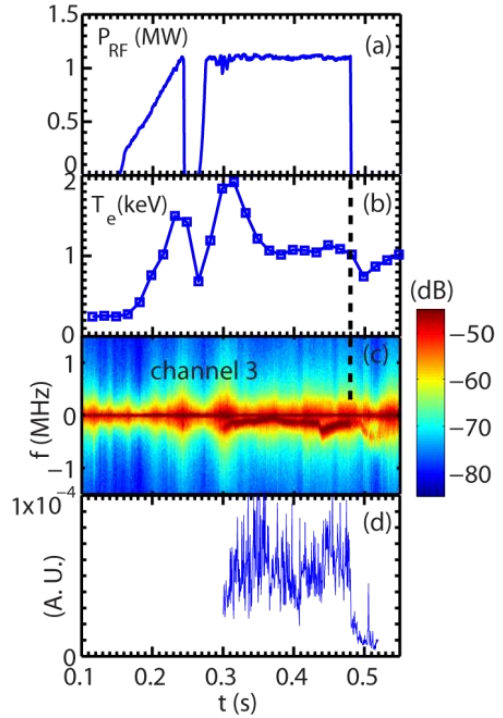


Figure 2 The time traces of (a) injected RF power and (b) maximum T_e ; (c) Spectrogram of signal from the channel 3 of the high- k scattering system; (d) Time trace of the peak spectral power of the scattered signal. The black vertical dashed line extends from (b) to (c) denotes the time point at which the RF heating is terminated, i.e. $t=479.6$ ms.

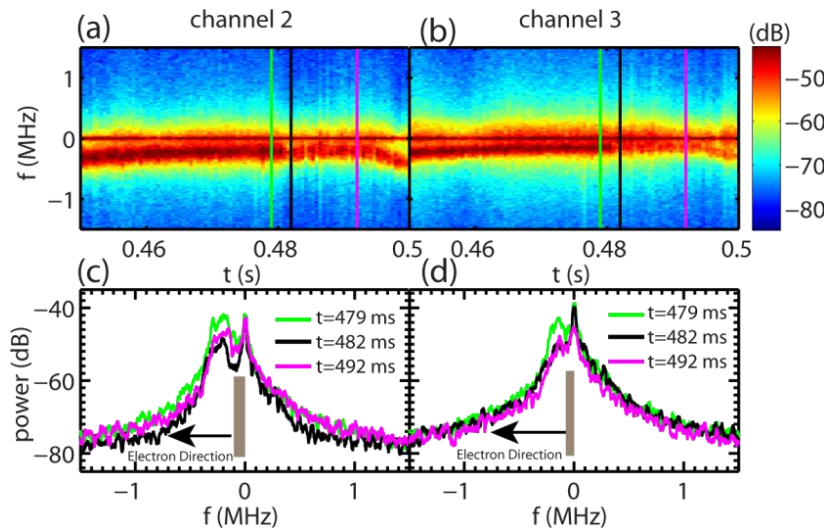


Figure 3 (a) and (b): The spectrograms of two high- k channels around the time of RF cessation, $t=479.6$ ms; (c) and (d): The frequency spectra at $t=479$ ms (green), 482 ms (black) and 492 ms (magenta) for the two high- k channels. The three color lines in the upper panels denote time points used for plotting the lower panels with the same color coding and the widths of the vertical grey bars in the lower panels denote the uncertainty of Doppler frequency shift. The electron direction is on the left hand side of the vertical grey bars in the lower panels.

power (at about $t=481$ ms) and the cessation of the RF heating (at $t=479.6$ ms) are not exactly synchronized: the drop in the spectral power happens approximately 1-2 ms after the RF cessation. The spectrograms also show that the drop in turbulence happens in about 0.5-1 ms, a time scale much faster than that on which one would expect equilibrium profiles to significantly vary. In fact, the typical energy confinement time for these kind of RF-heated L-mode plasmas is about 10 ms. Thus we would like to emphasize that the observed fast reduction of turbulence spectral power is unlikely due to any change in equilibrium profiles. We will further support this with equilibrium measurements later in the paper. More quantitative evaluation of the drop in turbulence spectral power can be seen Fig. 3(c) and (d). It is clear that after the sudden drop in spectral power, the turbulence remains a little changed from $t=482$ to 492 ms. The propagation direction of measured turbulence provides us clues about the nature of the turbulence. Plasma toroidal velocity is measured with charge exchange recombination spectroscopy (CHERS) measurements [19] with neutral beam blips (not shown). Measurements and analysis show that plasma toroidal velocity in the high- k measurement region at the time of RF cessation is very small ($\lesssim 5$ km/s), and this toroidal velocity gives us a Doppler frequency shift less than 100 kHz for channel 2 and less than 70 kHz for channel 3 [see the vertical grey bars shown in Fig. 3(c) and (d)]. Thus the frequencies at turbulence spectral peaks seen in Fig. 3 (c) and (d), about 150-200 kHz for channel 2 and 100-200 kHz for channel 3, can be easily separated from the Doppler shift frequencies. As we noted in Fig. 3(c) and (d), this separation allows us to determine the propagation direction of measured turbulence to be in the electron diamagnetic drift direction. Thus the observed turbulence has the propagation direction consistent with ETG turbulence. We will show later in the paper that ETG modes are indeed unstable in the high- k measurement region.

A closer examination of the temporal evolution of the measured high- k turbulence is shown in Fig. 3. Spectrograms of scattering channels 2 and 3 are shown in Fig. 3(a) and (b), respectively, and frequency spectra at three different time points, $t=479$ (right before the time of the RF cessation at $t=479.6$ ms), 482 and 492 ms are plotted in Fig. 3(c) (for channel 2) and (d) (for channel 3) (We note that channels 2 and 3 measure normalized wavenumbers $k_{\perp}\rho_s$ of 7-8 and 4-5, respectively). Now it is easy to determine the time of the sudden drop in turbulence spectral power from Fig. 3(a) and (b) to be about $t\approx 481$ ms. We also find that this sudden drop in the turbulence spectral

Since the high- k scattering system has five channels, we can further explore the change in wavenumber spectrum corresponding to the RF cessation (only four channels are used in the analysis since channel 5 was partially blocked by the vacuum vessel and also dominated by stray radiation). In Fig. 4, the wavenumber spectra at $t=479$ ms (at about the RF cessation and before the sudden drop in spectral power seen in Fig. 2), 484 and 492 ms (after the RF cessation and the sudden drop of turbulence) are shown (the wavenumber spectra was averaged over 3 ms around the denoted time points). Note that although after the RF cessation the turbulence spectral power varies little from $t=484$ to 492 ms, the drop in the spectral power is up to about a factor of 7 from $t=479$ ms (at the RF cessation) to 484/492 ms (after the RF cessation). We note that the drop seems to happen only at lower wavenumbers, namely $k_{\perp}\rho_s \lesssim 9$, which suggests that these longer wavelength modes may be more responsible for driving electron thermal transport for this discharge. It is

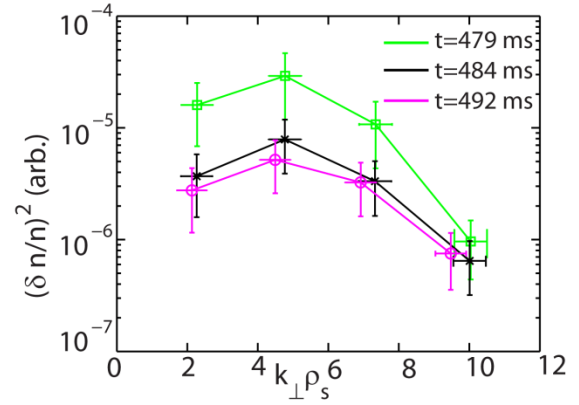


Figure 4 The local k spectra at $t= 479$ ms (green open square, before RF cessation), 484 (black asterisk, after RF cessation) and 492 ms (magenta open circle, after RF cessation) in the high- k measurement region.

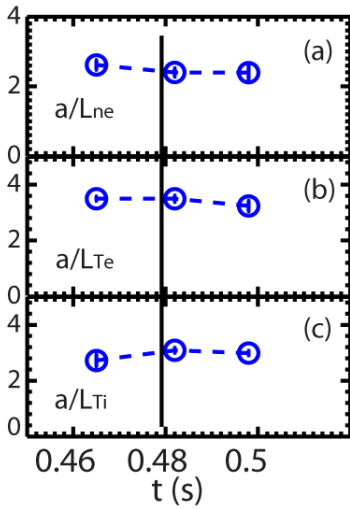


Figure 5 The temporal evolution of local normalized electron density, T_e and T_i gradients (a/L_{n_e} , a/L_{T_e} and a/L_{T_i}) averaged in the high- k measuring region at three exact Thomson measurement time points ($t=465$, 482 and 498 ms) in the high- k measurement region. The vertical solid line denotes the time of the RF cessation. Note that all gradients are normalized to a , the half width of last closed flux surface at mid-plane.

interesting to note that similar observations, i.e. longer wavelength modes better correlated with electron thermal transport, have been made in both neutral beam heated L and H-mode plasmas in NSTX (see Ref. [13,20]). Whether these observations have the universality they imply will require further experimental and numerical investigations.

As we mentioned before, the 0.5-1 ms time scale on which the turbulence spectral power drops is much smaller than the confinement time (~ 10 ms). Thus the local equilibrium profiles are not expected to significantly change on this time scale, and the observed sudden drop in turbulence spectral power is unlikely due to variations in local equilibrium gradients. Profile measurements shown in Fig. 5 support this argument. Figure 5 shows the normalized density, T_e and T_i gradients [a/L_{n_e} (a), a/L_{T_e} (b) and a/L_{T_i} (c)] averaged in the high- k measuring region at three exact time points of Thomson scattering measurements ($t=465$, 482 and 498 ms). Only small temporal variations ($\sim 15\%$) from $t=465$ to 498 ms are seen for the normalized gradients (variation in other equilibrium quantities is similar). We note that the second Thomson time point, $t=482$ ms, is after the RF cessation and also right after the sudden drop in measured turbulence at $t\approx 481$ ms. We emphasize that although the first Thomson time point, $t=465$ ms, is separated by 17 ms from the second Thomson time point, $t=482$ ms, the gradient variation between the two time points seen in Fig. 5 is still small. This strongly suggests that the equilibrium profiles at $t=465$ ms may be able to represent the profiles right before the RF cessation. Furthermore, the 15% variation in the equilibrium gradients over 17 ms (from 465 to 482 ms) also

strongly suggests that the variation in gradients on the 0.5-1 ms time scale should be $\ll 15\%$.

Electron thermal transport was evaluated with TRANSP transport analysis code [21] coupled with TORIC calculation for the RF heating profile [22]. The amount of RF power coupled into the plasma is estimated by evaluating the peak increasing rate of total stored energy at the RF turn-on phase (from $t=265$ to 300 ms) and it shows that an approximate 30 percent of the total RF power is coupled into the plasma. This estimation assumes that thermal transport does not change significantly in the RF turn-on phase and this assumption is partly supported by the fact that no significant scattering signal is seen from $t=265$ to 300 ms [see Fig. 2(c)]. The electron thermal diffusivity, χ_e , profiles at two exact Thomson measurement time points ($t=465$ and 482 ms) as used in Fig. 5 are shown in Fig. 6 where a factor of 2 decrease in χ_e can be seen after the RF cessation at $t=482$ ms. Such a drop in χ_e is correlated with the sudden drop in electron-scale turbulence spectral power shown in Fig. 4 but not correlated with the variations in the local equilibrium gradients as we have shown in Fig. 5, demonstrating the nonlocal nature of the observed turbulence and electron thermal transport.

In order to explore instabilities operating in the high- k measurement region in these RF-heated L-mode plasmas, linear stability analysis was performed with the GS2 gyrokinetic code [23]. GS2 is an initial value gyrokinetic code which, in its linear mode, finds the fastest growing mode for a given pair of poloidal and radial wavenumbers. The linear analysis was carried out from the ion scale ($k_\theta \rho_s \lesssim 1$) to the electron scale ($k_\theta \rho_e \sim 0.5$). Figure 7(a) shows that a wide k_θ range of linear modes is seen to be unstable with maximum linear growth rate,

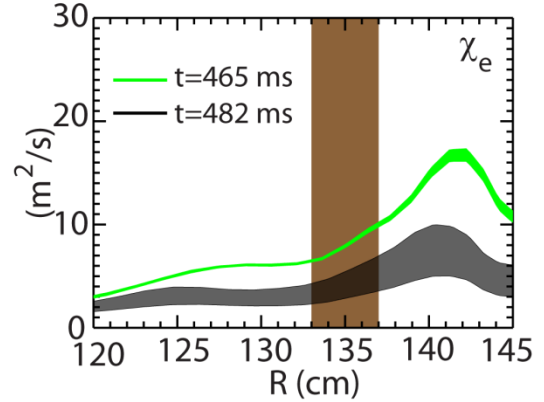


Figure 6 Electron thermal diffusivity, χ_e , at $t=465$ ms (about 14 ms before RF cessation) and 482 ms (after RF cessation) plotted as colored bands with vertical width denoting standard deviation. The rectangular shaded region denotes the measurement region of the high- k scattering system.

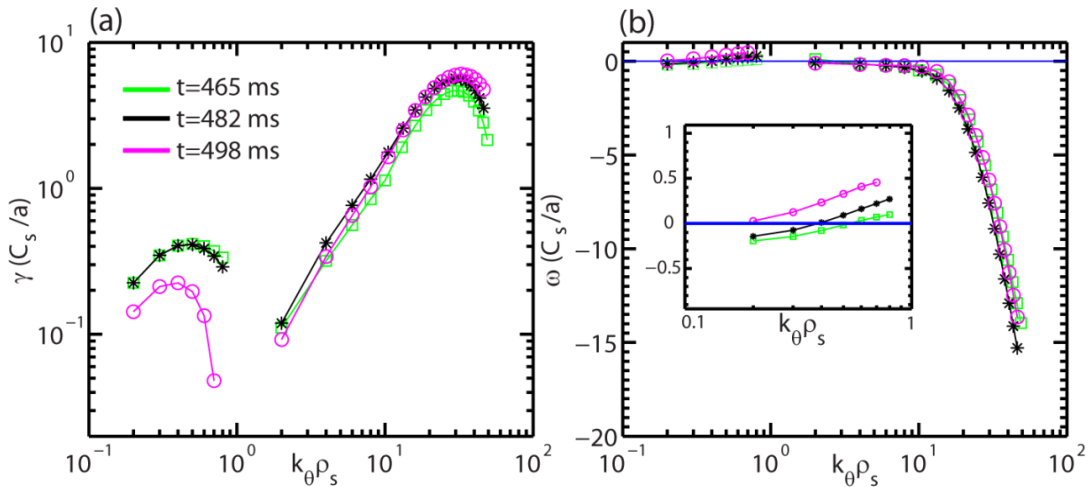


Figure 7 (a) Linear growth rate, γ , and (b) mode frequency, ω , spectra at $t=465$ ms (green open square), $t=482$ ms (black asterisk) and $t=498$ ms (magenta open circle) calculated with GS2 code at $R=135$ cm ($r/a=0.6$ about the center of the high- k measurement region) using local Miller equilibrium. Note that modes with $\omega < 0$ propagate in the electron diamagnetic drift direction and $\omega > 0$ denotes the ion diamagnetic drift direction. The insert in (b) shows a zoomed-in portion of the real frequency spectra in the ion scale (from $k_\theta \rho_s = 0.1$ to 1).

γ , ranging from about 0.2-0.4 C_s/a at ion scale to 5-6 C_s/a at electron scale at the three exact Thomson time points as used in Fig. 5. The wave propagation direction seen in Fig. 7(b) provides the information on the nature of the modes. It can be seen that the ion-scale modes can propagate in the ion diamagnetic direction and/or the electron diamagnetic direction [see the insert in Fig. 7(b)], showing that the ion-scale modes are hybrid modes driven by both electron and ion temperature gradients. In fact, further linear analysis shows that a critical ion or electron temperature gradient cannot be determined by varying either of them alone. This result will be presented in a future full paper. Electron-scale modes propagate in the electron direction and are identified as ETG modes. Comparing the ETG linear growth rates among the three time points, we find that the maximum ETG linear growth rate slightly increases from about 5 C_s/a at $t=465$ ms to about 6 C_s/a at $t=498$ ms. This increase, however, is not consistent with observed decrease in electron-scale turbulence as seen in Fig. 3 and Fig. 4. In particular, the sudden drop in the turbulence spectral power cannot be explained by the tiny change in the ETG linear growth shown in Fig. 7(a). The maximum ion-scale linear growth rate seen Fig. 7(a), on the other hand, shows almost no change from $t=465$ to 482 ms, which is obviously inconsistent with the drop in measured electron-scale turbulence if we consider the possible nonlinear interaction between ion-scale and electrons-scale turbulence as suggested in Ref. [20,24]. We note that there is a factor of about 2 drop in maximum ion-scale linear growth rate at $t=498$ ms compared with those at the earlier two time points. Further linear analysis shows that this is due to a small decrease in a/L_{T_e} and a small increase in T_i/T_e from $t=482$ to 498 ms. Furthermore, due to the small toroidal rotation mentioned above ($\lesssim 5$ km/s), the ExB shearing rate from $t=465$ to 498 ms is small, $\lesssim 0.03 C_s/a$ (evaluated using the Waltz-Miller ExB shearing rate [25]) which is much smaller than the maximum ion-scale linear growth rates shown in Fig. 7(a), $\gtrsim 0.2 C_s/a$. Thus the ExB shear cannot significantly affect ion-scale turbulence. Finally, we emphasize that the decrease in maximum ion-scale linear growth rate from $t=482$ to 498 ms does not affect our conclusion that the change in linear growth rates cannot explain the observed significant drop in electron-scale turbulence at the RF cessation even if we take into account the plausible nonlinear coupling between ion-scale and electron-scale turbulence [20,24].

We have also used GS2 code to determine the linear critical a/L_{T_e} and a/L_{T_i} for the ion-scale hybrid modes and ETG modes. The results shows that both modes are far from marginal stability and are robustly unstable before and right after the RF cessation in these plasmas. We will present this analysis in full in a future paper. We would like to conclude that the above analysis shows the linear stability framework cannot explain the observed reduction in electron-scale turbulence at the RF cessation.

4. Discussions and Summary

In summary, we present the first experimental observation of nonlocal electron thermal transport in a set of NSTX RF-heated L-mode plasmas. The results clearly shows that a time delay of about 1-2 ms between the RF cessation and the drop in measured electron-scale turbulence, indicating a causal relation between the two. We also show that the drop in turbulence spectral power happen on a 0.5-1 ms time scale, which is too fast for the standard local transport paradigm to provide satisfying explanations. This is because while the reduction of turbulence can happen on a small time scale as we observed in the experiment, the changes in the local equilibrium profiles on this time scale remain negligible since the equilibrium varies on the much-longer confinement time scale. However, the observation is intuitively consistent with a picture of flux-driven turbulence: a decrease in heat flux leads to a decrease in turbulence responsible for thermal transport. Power balance analysis has shown a factor of about 2 decrease in electron thermal diffusivity after the sudden drop of measured

turbulence. We note that a recent theoretical work has provided a nice foundation for the flux-driven turbulence [26]. Furthermore, the linear stability analysis presented here has demonstrated that both ion-scale and electron-scale instabilities are unstable in the high- k measurement region. However, the change in linear growth rates from equilibrium variations fails to provide a consistent explanation of the experimental observations. We would like to point out that extreme profile stiffness is needed to explain the experimental observation due to the expected small changes in the local equilibrium profiles (and gradients) on the turbulence changing time scale (0.5-1 ms). We have carried out gradient-driven nonlinear gyrokinetic simulations to assess profile stiffness in these plasmas, and the results show that the electron temperature profile is far from stiff, i.e. a 25% increase in ETG only leads to 18% increase in electron heat flux. We note that the electron temperature profile stiffness reported in the literature [27, 28], where $\geq 15\%$ variation in ETG is needed to change electron heat flux by a factor of 2, is also insufficient to explain the observation in this paper, i.e. a factor of about 2 reduction in electron heat flux with a variation in ETG $\ll 15\%$. Furthermore, we will explore the nonlocal effects using global gyrokinetic code, i.e. GTS [29].

Acknowledgements: This work was supported by U.S. Dept. of Energy contracts No. DE-AC02-09CH11466, No. DE-FG03-95ER54295, and No. DE-FG03-99ER54518.

References:

- [1] J. E. Menard et al., Nuclear Fusion 51, 103014 (2011).
- [2] K. W. Gentle et al., Phys. Rev. Lett. 74, 3620 (1995).
- [3] N. Tamura et al., Fusion Sci. & Tech. 58, 122 (2010).
- [4] C. Gao et al., Nucl. Fusion 54, 083025 (2014).
- [5] K. Ida, private communication.
- [6] W. Dorland et al., Phys. Rev. Lett. 85, 5579 (2000).
- [7] Y. Ren et al., Phys. Rev. Lett. 106, 165005 (2011).
- [8] W. Guttenfelder and J. Candy, Physics of Plasmas 18, 022506 (2011).
- [9] S. M. Kaye et al., Nucl. Fusion 47, 499 (2007).
- [10] D. R. Smith et al., Rev. Sci. Instrum. 79, 123501 (2008).
- [11] E. Mazzucato, Phys. Plasmas 10, 753 (2003).
- [12] E. Mazzucato et al., Phys. Rev. Lett. 101, 075001 (2008).
- [13] Y. Ren et al., Physics of Plasmas 19, 056125 (2012).
- [14] H. Y. Yuh et al., Phys. Rev. Lett. 106, 055003 (2011).
- [15] E. Mazzucato et al., Nuclear Fusion 49, 055001 (2009).
- [16] M. Ono et al., Nuclear Fusion 40, 557 (2000).
- [17] B. P. LeBlanc et al., Rev. Sci. Instrum. 74, 1659 (2003).
- [18] B. LeBlanc et al., Nuclear Fusion 44, 513 (2004).
- [19] R. E. Bell, Rev. Sci. Instrum. 77, 10E902 (2006).
- [20] Y. Ren et al., Nuclear Fusion 53, 083007 (2013).
- [21] R. J. Hawryluk, Physics of Plasma Close to Thermonuclear Conditions (Pergamon, New York, 1981).
- [22] M. Brambilla, Plasma Phys. Cont. Fusion 41, 1 (1999).
- [23] M. Kotschenreuther et al., Comp. Phys. Comm. 88, 128 (1995).
- [24] F. Jenko, J. Plasma Fusion Res. SERIE 6, 11 (2004).
- [25] R. E. Waltz and R. L. Miller, Physics of Plasmas 6, 4265 (1999).
- [26] S.-I. Itoh and K. Itoh, Sci. Rep. 2, 860 (2012).
- [27] J. C. Hillesheim et al., Phys. Rev. Lett. 110, 045003 (2013).
- [28] J. L. Peterson et al., Physics of Plasmas 19, 056120 (2012).
- [29] W.X. Wang et al., Phys. Plasmas, 17, 072511 (2010).